Fermilab-FN-1035-APC
September 2017

MODELING RADIATION LOADS IN THE ILC MAIN LINAC AND A NOVEL APPROACH TO TREAT DARK CURRENT

Nikolai V. Mokhov, Igor L. Rakhno†, Igor S. Tropin
Fermi National Accelerator Laboratory, Batavia, Illinois 60510, USA

Abstract

Electromagnetic and hadron showers generated by electrons of dark current (DC) can represent a significant radiation threat to the ILC linac equipment and personnel. In this study, a commissioning scenario is analysed which is considered as the worst-case scenario for the main linac regarding the DC contribution to the radiation environment in the tunnel. A normal operation scenario is analysed as well. An emphasis is made on radiation load to sensitive electronic equipment—cryogenic thermometers inside the cryomodules. Prompt and residual dose rates in the ILC main linac tunnels were also calculated in these new high-statistics runs. A novel approach was developed—as a part of general purpose Monte Carlo code MARS15—to model generation, acceleration and transport of DC electrons in electromagnetic fields inside SRF cavities. Comparisons were made with a standard approach when a set of pre-calculated DC electron trajectories is used, with a proper normalization, as a source for Monte Carlo modelling. Results of MARS15 Monte Carlo calculations, performed for the current main linac tunnel design, reveal that the peak absorbed dose in the cryogenic thermometers in the main tunnel for 20 years of operation is about 0.8 MGy. The calculated contact residual dose on cryomodules and tunnel walls in the main tunnel for typical irradiation and cooling conditions is 0.1 and 0.01 mSv/hr, respectively.

†rakhno@fnal.gov

This manuscript has been authored by Fermi Research Alliance, LLC under Contract No. DE-AC02-07CH11359 with the U.S. Department of Energy, Office of Science, Office of High Energy Physics.

Introduction

It has been recognized in numerous studies [1-5] that the loss of dark current (DC) generated in the superconducting RF (SRF) cavities is the dominant source of radiation loads on the ILC Main Linac components and related radiation environment in the tunnel. The DC-induced loads are several orders of magnitude higher than those induced by beam-gas Coulomb scattering and beam-gas bremsstrahlung [5]. Radiation studies related to DC generated in the ILC SRF cavities for both normal operation and commissioning are described in detail in [6]. That work was focused on prompt dose distributions in both the main linac and service tunnels. In this study, the emphasis is made on radiation load to sensitive electronic equipment—cryogenic thermometers inside the cryomodules—in terms of absorbed dose and 1-MeV neutron equivalent fluence. Distributions of prompt and residual dose over both the tunnel and cryomodule cross sections are calculated and presented as well. The calculation results are given for both the normal operation and commissioning.

In a standard approach, a set of pre-calculated DC electron trajectories [6] is used as a source for subsequent Monte Carlo modelling. In order to normalize the calculations, the source was prepared assuming that the contribution to DC from every single SRF cavity is equal to 50 nA.

Then, a novel approach was developed—as a part of general purpose Monte Carlo code MARS15 [7,8]—to model generation, acceleration and transport of DC electrons in electromagnetic (EM) fields inside SRF cavities. Comparisons were made with a standard approach with a corresponding normalization. From these comparisons, the calculated dose distributions are close in both the cases, and the problem of a proper normalization of DC remains a non-trivial issue.

MARS15 geometry model

A cross section of the ILC Kamaboko tunnel is shown in Figure 1. In the current design, there is a wall between main and service tunnels. Thickness of this wall (1.5-3.5 m), that separates the service and operational parts of the tunnel, is determined by the maximum beam losses. It was shown in [6] that the design dose level of 25 μSv/hr is reached after 2.2 m of the concrete wall.

Figure 1: A cross section of ILC Kamaboko tunnel (the dimensions are given in mm)

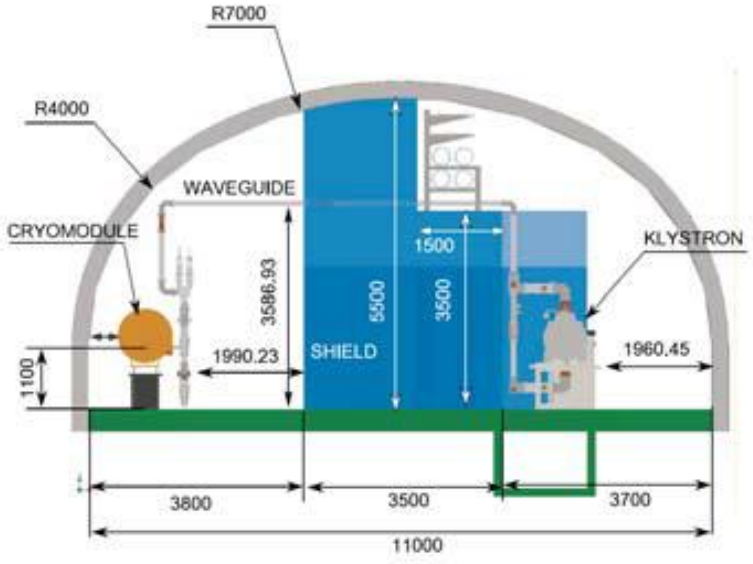

Several fragments of the MARS15 geometry model are shown in Figure 2. The current model provides quite realistic description of the ILC main linac with major beam components in both main and service tunnels. The Cernox cryogenic thermometers [9] were modelled as thin cylindrical layers on the three pipes inside the cryo-module as shown in Figure 3. The following energy thresholds were used in our calculations: 10^{-3} eV for neutrons and 0.1 MeV for all other particles.

Figure 2: Fragments of the MARS15 model – tunnel cross section (top left), 9-cell SRF cavity (top right), cryo-module elevation view with an SRF cavity and cross section with a quadrupole magnet (bottom left and right, respectively)

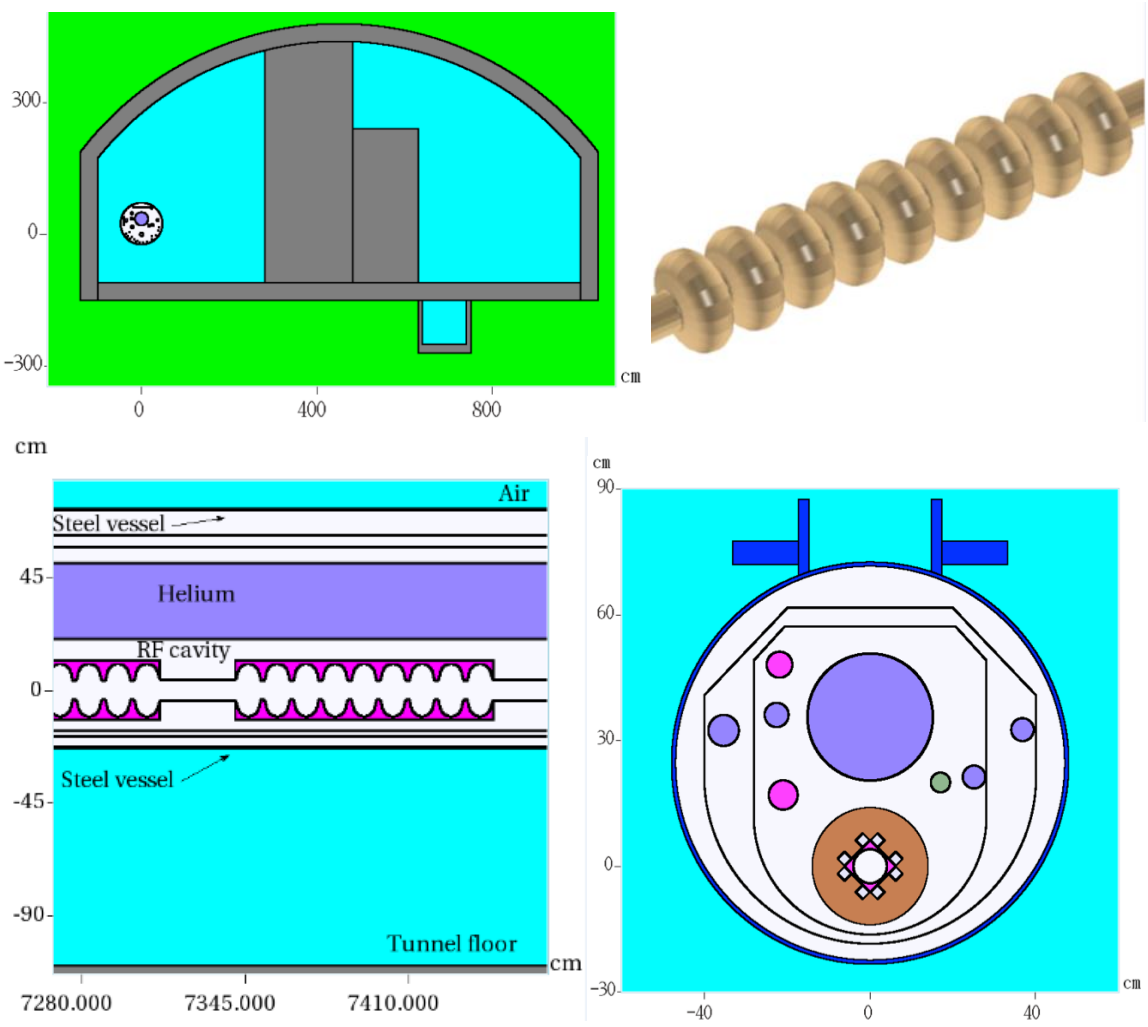

Modes of operation

First, we considered a normal mode of operation of the linac, when RF power to both the cavities and quadrupole magnets is turned on. Also studied is the worst-case commissioning mode of operation when only RF power to the cavities is turned on, while quadrupole magnets are turned off.

It was found in our previous study [6] that such a commissioning mode is more severe from the standpoint of prompt radiation.

Figure 3: A cross section of a cryo-module in the MARS15 model. The Cernox cryogenic thermometers are modelled as thin cylindrical layers on the three pipes shown by arrows.

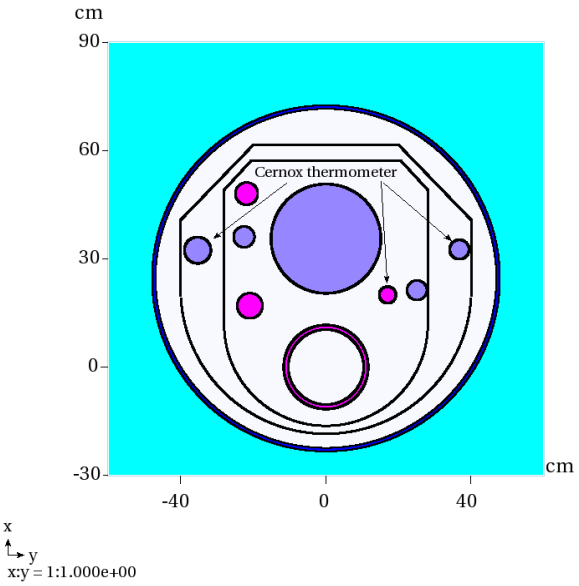

Normal operation

In the normal mode of operation, the DC electrons are lost mostly on the magnets and nearest cavities downstream. The maximum energy of the lost DC electrons can be as high as 828 MeV [6]. In this case, the equilibrium state, when losses of DC particles along the linac are compensated by newly generated DC electrons, is reached already at the second RF unit. The largest losses in this mode are observed at the end of the linac and concentrated at the locations of focusing magnets and nearest cavities downstream. Figure 4 shows the distribution of both the prompt and residual dose over the tunnel cross section at the first SRF cavity immediately downstream of the last focusing magnet at the end of linac. The highest prompt dose in the service tunnel near the 2-m thick concrete wall section is 0.5 µSv/hr. Thus, in the current design of the ILC main linac and in the normal mode of operation, the concrete wall between main and service tunnels provides a safety factor of about 50 for radiation protection. The predicted contact residual dose on the main tunnel concrete walls does not exceed 10 µSv/hr.

More detailed distributions of prompt and residual dose over a cryo-module cross section are shown in Figure 5, while Figure 6 shows the distribution of the 1-MeV neutron equivalent flux, the quantity widely used as a merit of radiation damage to sensitive electronic equipment. The peak calculated absorbed dose and 1-MeV neutron equivalent fluence in the Cernox cryogenic thermometers are observed in the very first cavity downstream of the quadrupole, and corresponding numerical values are given in Table 1. One can see that the highest predicted residual dose, 0.95 mSv/hr, is inside the quadrupole. Note that the residual dose on contact shown in this paper represents well the reality for the concrete walls and other large objects, being an overestimation by a factor of up to 5 for thin pipes and small objects like thermometers. The structural elements located atop the cryomodule are activated significantly less, at the level of about a few µSv/hr.

The peak absorbed dose in the thermometers for 20 years of operation—0.76 MGy—looks high relative to the upper tested dose of 10 kGy [9] when the Cernox thermometers still exhibit high radiation hardness. However, the standard normalization used for the pre-calculated DC source—50 nA from each cavity—is quite conservative. Therefore, a proper re-evaluation of the normalization is needed which can be a subject of another study.

Figure 4: Prompt (left) and residual (right) dose (mSv/hr) over the tunnel cross section at the end of the ILC main linac for normal operation. The residual dose on contact was calculated for a 100-day operation and 4-hour cooling scenario.

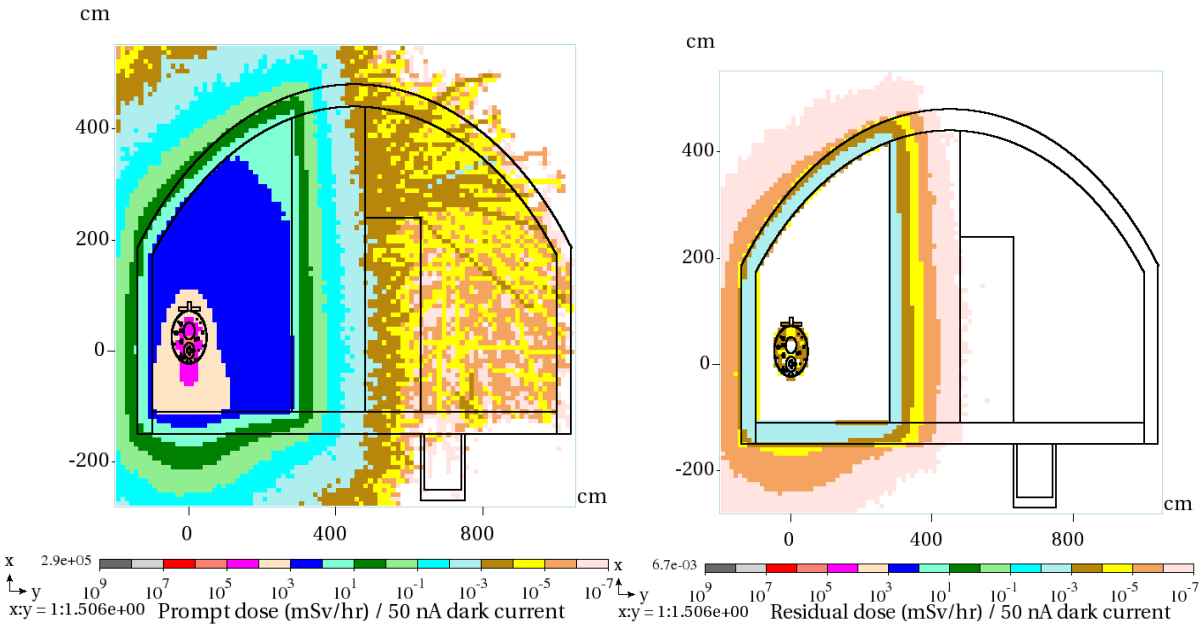

Figure 5: Prompt (left) and residual (right) dose (mSv/hr) in a cryo-module cross section at the last quadrupole. The residual dose on contact was calculated for a 100-day operation and 4-hour cooling scenario.

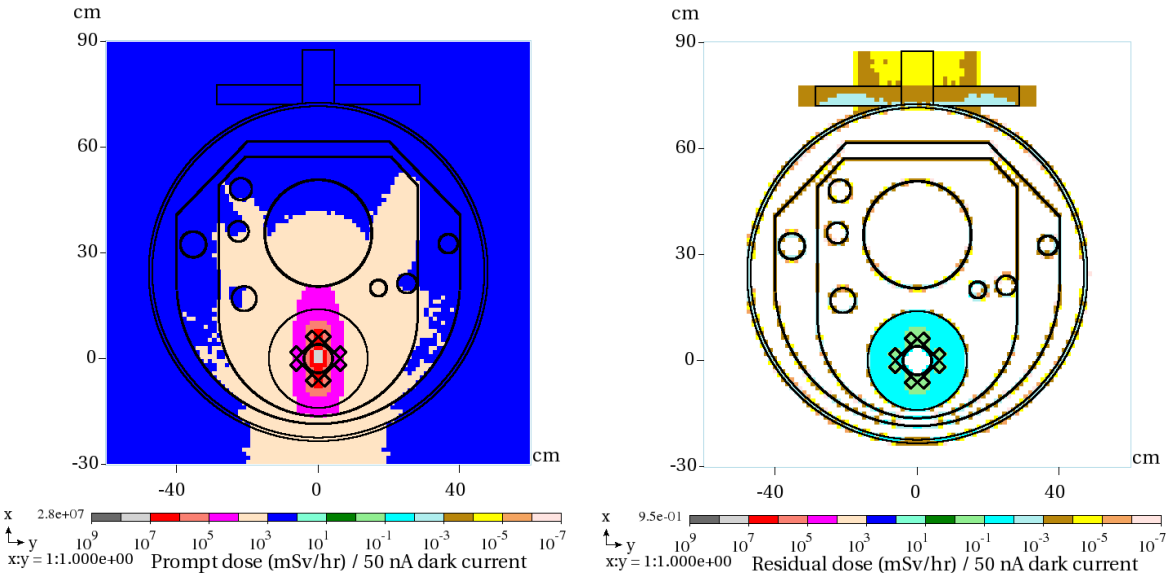

Table 1. Peak absorbed dose (DAB) and 1-MeV neutron equivalent fluence (EQ1) **after 20 years of operation** predicted in the first SRF cavity immediately downstream of the last quadrupole. It is assumed that an operational year contains 10^7 seconds. The locations 1, 2 and 3 correspond to the Cernox thermometer locations shown in Figure 3 when counting from left to right.

	Location 1	Location 2	Location 3
DAB (MGy)	0.24	0.76	0.10
EQ1 (10^{13} n/cm^2)	5.2	11.0	2.7

Figure 6: 1-MeV neutron equivalent flux over a cryo-module cross section at the last quadrupole.

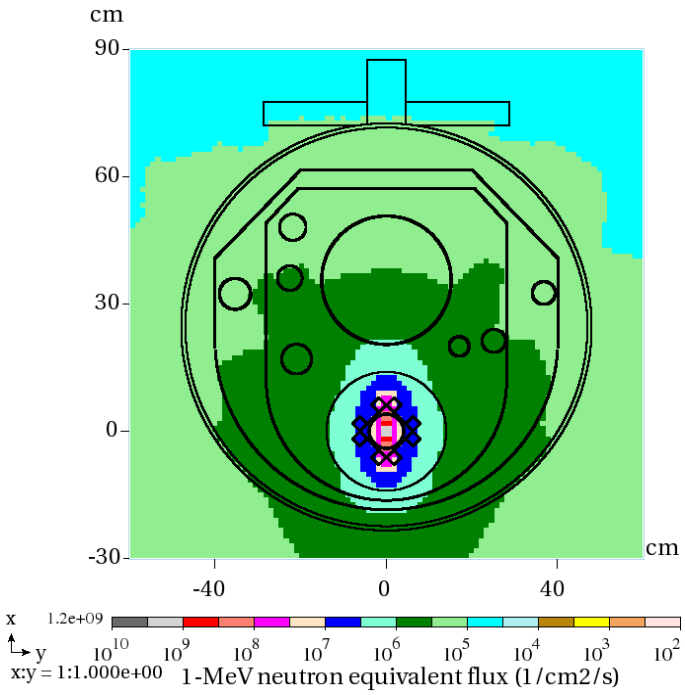

The worst-case commissioning mode

Turning off quadrupole magnets while still having RF power in cavities can, potentially, present worse conditions from standpoint of radiation generated around the linac when comparing to the normal mode of operation described above. When quads are turned off, DC electrons can traverse many RF units of linac and get accelerated up to high energies before they hit a material and generate showers of secondary particles. It follows from our previous study [6] that **the worst case** is the following option—**a curved linac with steering magnets ON and correction ON for misalignment**.

The calculated results in this section are given for this worst-case commissioning scenario. In Figure 7 we compare prompt dose distributions for normal operation and the worst-case mode, and Figure 8 shows residual dose for the worst-case mode. Figures 9 and 10 provide prompt and residual dose and 1-MeV neutron equivalent flux over a cross section of a cryomodule. Peak values of radiation damage to the Cernox cryogenic thermometers in terms of absorbed dose and 1-MeV neutron equivalent fluence are presented in Table 2.

Figure 7: Prompt dose (mSv/hr) for normal operation (left) and the worst-case commissioning mode (right) of the ILC main linac.

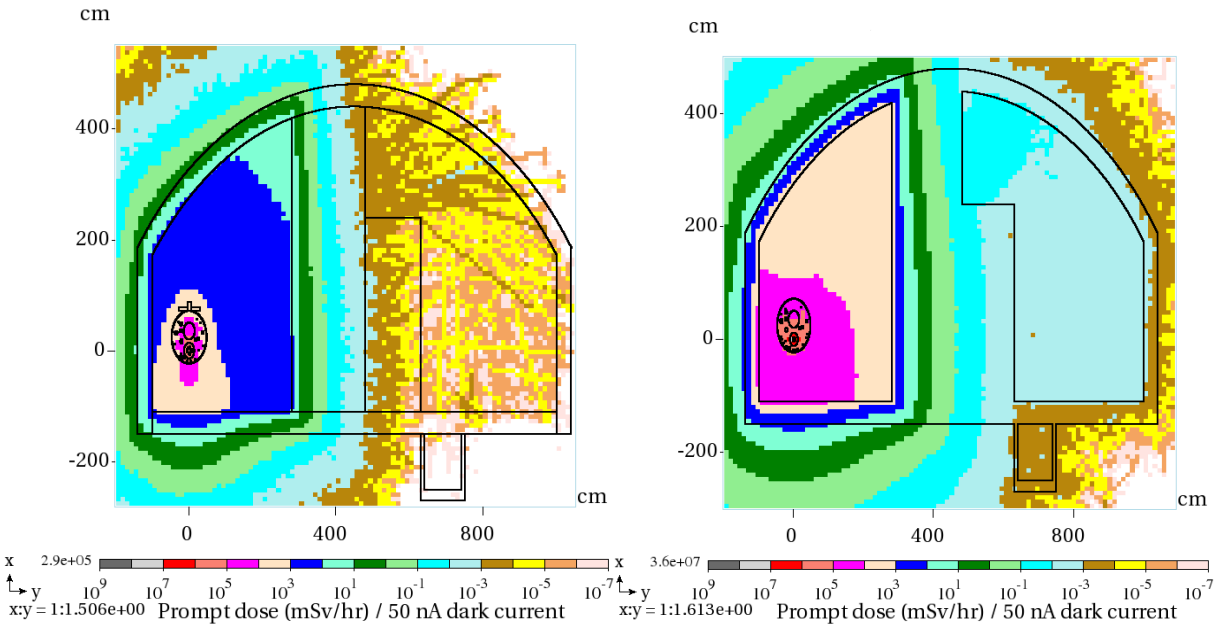

Figure 8: Residual dose (mSv/hr) on contact over a cross section of the ILC main linac tunnel calculated for a 100-day operation and 4-hour cooling scenario for the worst-case mode.

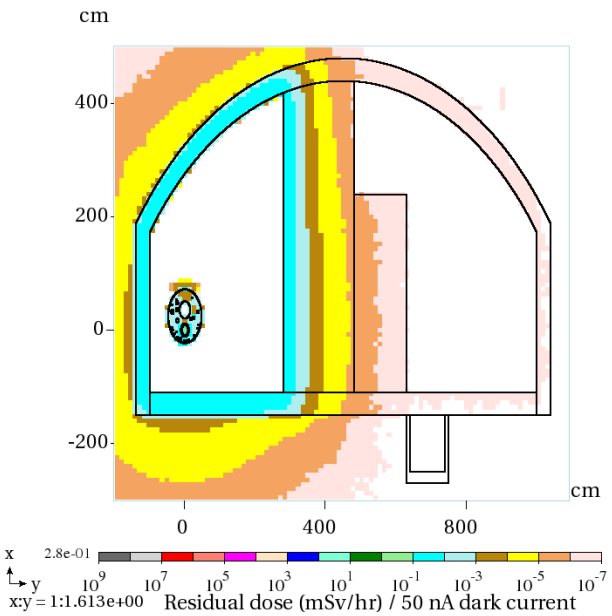

Figure 9: Prompt (left) and contact residual (right) dose (mSv/hr) in a cryo-module cross section of the ILC linac. The residual dose was calculated for a 100-day operation and 4-hour cooling scenario for the worst-case commissioning mode.

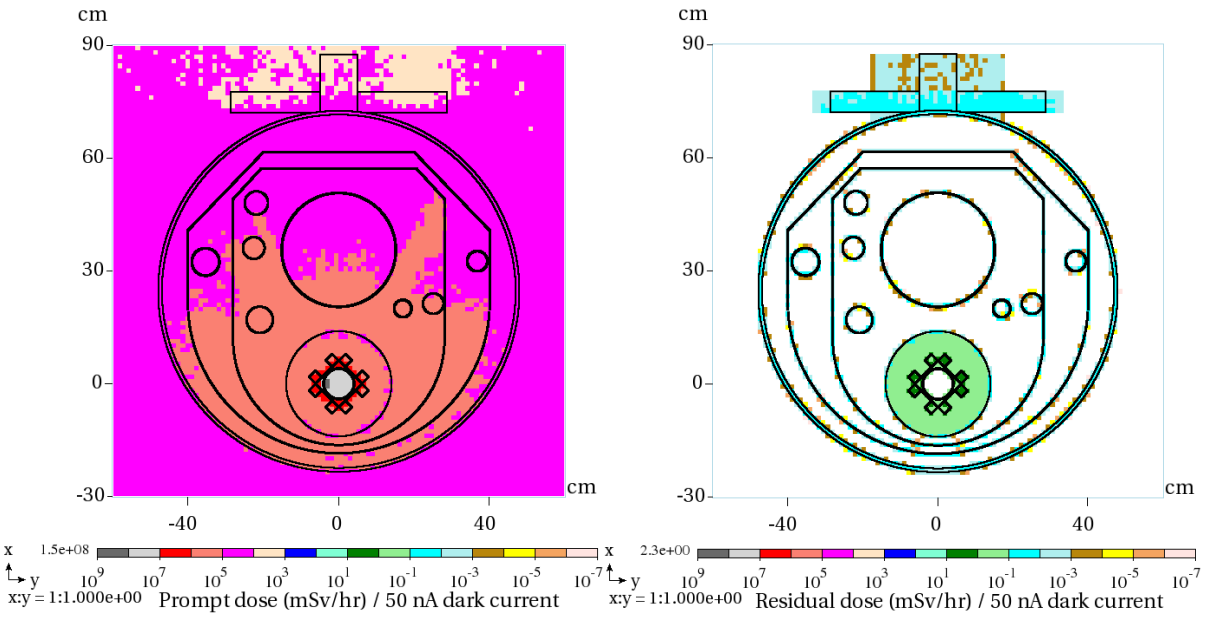

Figure 10: 1-MeV neutron equivalent flux over a cryo-module cross section for the worst-case commissioning mode.

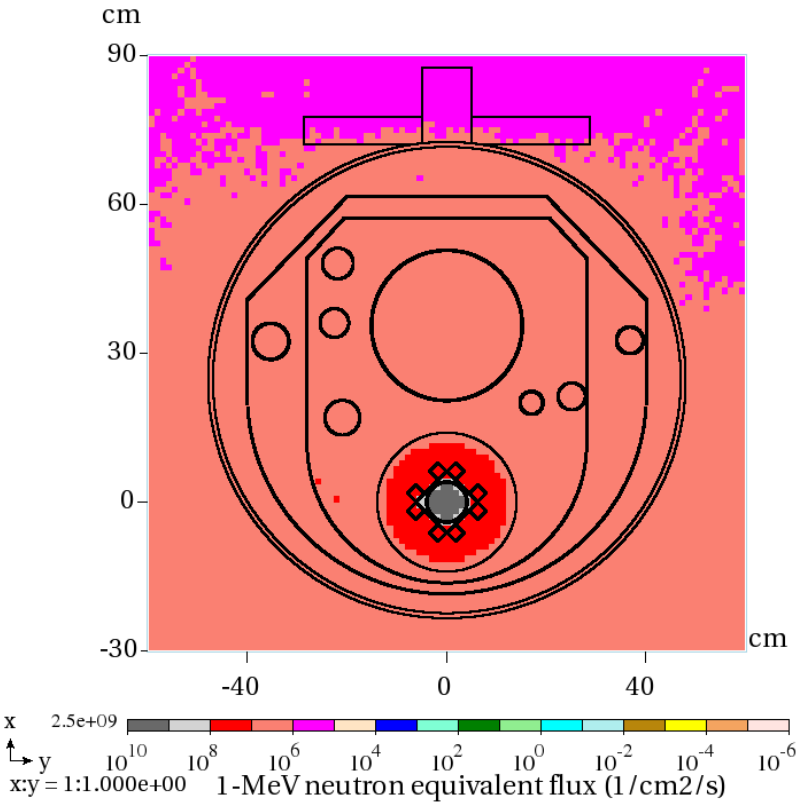

Table 2. Peak absorbed dose (DAB) and 1-MeV neutron equivalent fluence (EQ1**) after 6 months of the worst-case commissioning** predicted in SRF cavities. It is assumed that an operational year contains 10^7 seconds. The locations 1, 2 and 3 correspond to the Cernox thermometer locations shown in Figure 3 when counting from left to right.

	Location 1	Location 2	Location 3
DAB (MGy)	0.073	0.17	0.052
EQ1 (10^{13} n/cm^2)	1.34	2.45	1.08

Generation of DC electrons on SRF cavity surface

Distribution of DC electrons generated on the inner SRF cavity surface is described by the expression initially derived by Fowler and Nordheim [10]. Afterwards some corrections have been made to the expression. In this study, we employ the following simplified expression [11]:

$$J = a\phi^{-1}F^2 \exp\left[\frac{-v(f)b\phi^{3/2}}{F}\right], \qquad (1)$$

where J (A/m^2) is DC density, $a \approx 1.541434\times10^{-6}\ (AeVV^{-2})$, $F = E\,\beta$, E is time dependent electric field in the immediate vicinity of the cavity surface (V/nm); $\beta = 100$ is the field enhancement factor, $\phi = 4.2\ (eV)$ is the local work function, $f = 1.439964\ (eV^2V^{-1}nm)\ F/\phi^2$, v(f) ≈1-f+(1/6) f ln(f).

The expression (1) is applicable to an SRF cavity with the ideal surface in which case the field distribution inside the cavity is assumed to be well known. Various surface imperfections can significantly distort the field distribution which renders the expression (1) conditionally applicable. In the latter case one assumes that the functional dependence remains intact, but the field-independent pre-exponential factor is a normalization parameter that should be determined using separate considerations.

High-precision Runge-Kutta solver for electron acceleration and transport in EM fields

The calculations of acceleration and transport of generated DC electrons are carried out by means of the Dormand-Prince integrator with step size control and dense output. It performs numerical integration of the system of two time-dependent differential equations for coordinate and momentum. The integrator implementation is based on the approach described in [12] and on the boost::odeint library [13]. A boundary crossing algorithm was added as well. The time dependent electromagnetic field required for calculation of electric force was interpolated from the same 2D table [14] as used in [6]. The described solver is integrated in the MARS15 tracking algorithm and applicable to all charged particles entering a cavity from surrounding regions or created as a result of the field emission. Figure 11 shows calculated electron energy gain in the very last section of the ILC linac as well as several sample trajectories inside an SRF cavity.

Figure 11: Calculated electron energy gain in the very last section of ILC linac (top) and several sample electron trajectories in an SRF cavity (bottom).

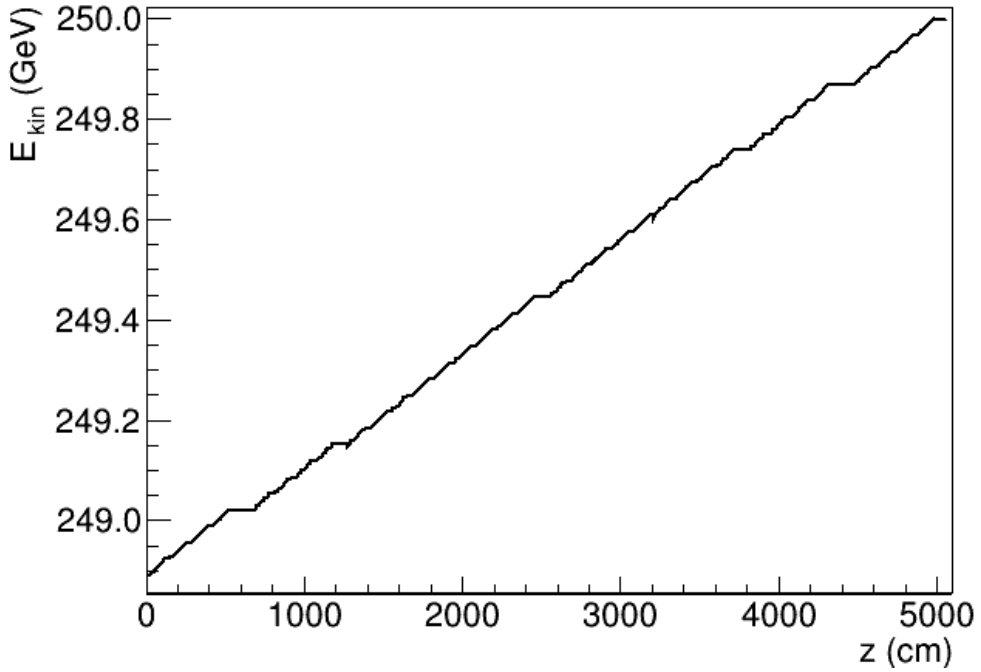

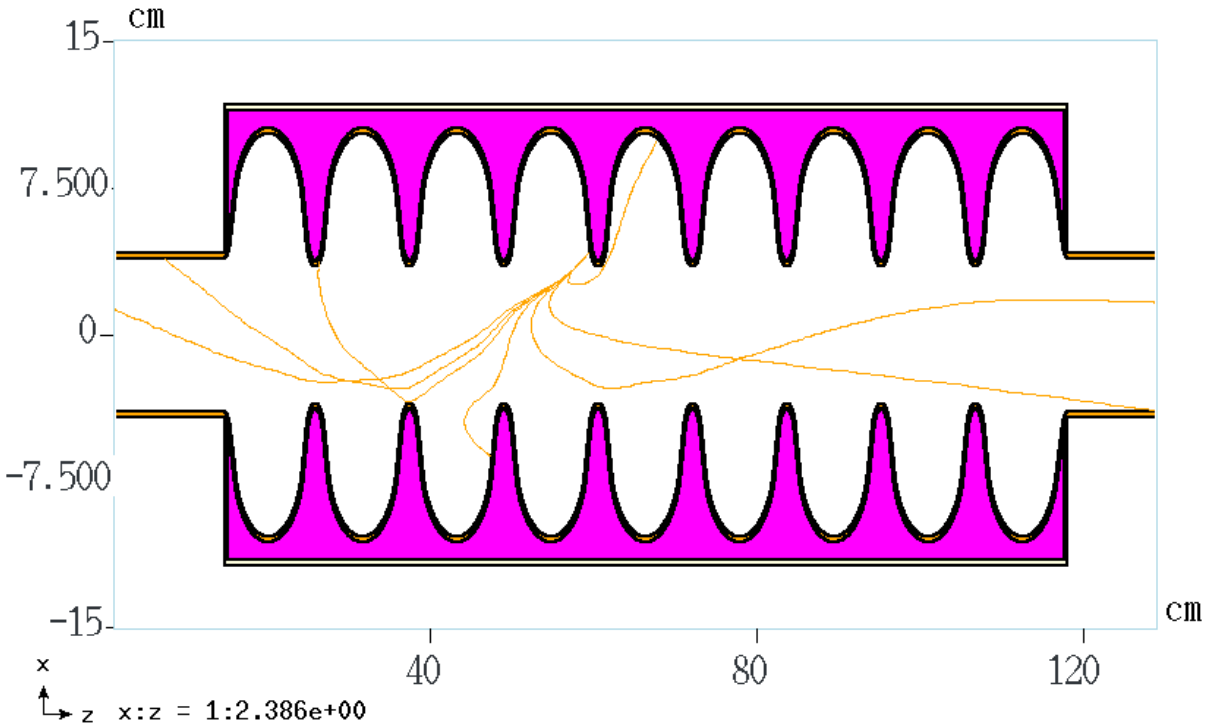

Calculations with the new solver

An analysis has shown that, in the case when field emission is described by formula (1) and emission points are distributed uniformly over the cavity surface, the forward DC from the cavity 30 toward quadrupole does not exceed 2.1 nA (see Figure 12), with the average current over the 30 cavities being approximately 1 nA. However, when dealing with realistic cavities with surface imperfections that can distort the local field significantly, the DC prediction is getting more uncertain. Therefore, in practice it is usually assumed that DC in every single cavity cannot exceed a certain value, and cavities which reveal DC above that level are rejected during a testing stage. In a previous study [6], the above-mentioned value was selected to be 50 nA. It appears to be conservative compared to the average current of 1 nA. However, if a cavity with significant surface imperfections is placed in the very beginning of such a beam line segment, DC in the last cavity of the segment can, probably, exceed the assumed level of 50 nA due to significant amplification shown in Figure 12. Therefore, a more elaborate scenario is needed in order to determine more reliable and detailed radiation environment around the ILC main linac tunnel, which can be a subject of further studies.

Results of calculations performed for **the normal operation case** with the newly developed solver are presented in Figures 13 and 14 for a beam line segment that contains the last four cryomodules of the main linac with 34 cavities and two quadrupole magnets, Q1 and Q2, located downstream of the cavities 4 and 30, respectively. One can see that a significant DC production and acceleration occurs in all the cavities between the quadrupoles which perform a cleaning function, so that only a small percentage of forward-peaked DC propagates farther downstream the beamline. Partial contributions to DC from different cavities are comparable but not equal. The energy spectrum of generated electrons—including the electron endpoint energy of about 840 MeV—is very close to that obtained in a traditional approach with pre-calculated external source. Figures 15 thru 18 show various distributions of prompt and absorbed dose calculated for the beam line segment.

Figure 12: Power (W) (left) and current (nA) (right) of accelerated DC electrons counted in the aperture at the downstream end of each cavity. The results include both field emitted electrons which did not experience any interaction with cavity walls and electrons that already experienced either elastic or inelastic scattering in cavity walls. The labels Q1 and Q2 indicate locations of quadrupole magnet 1 and 2, respectively.

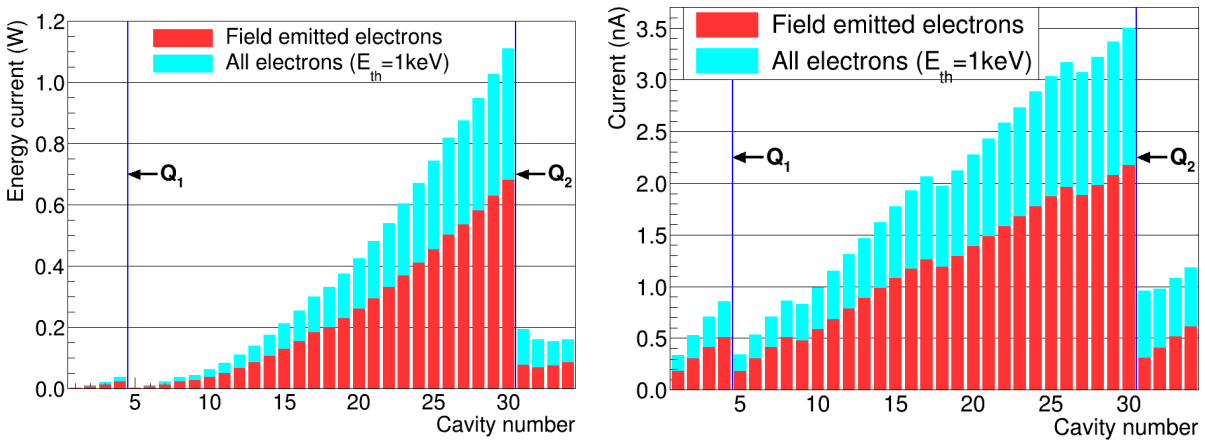

Figure 13: Energy spectra of DC electrons calculated with two different approaches (area under each histogram is equal to 1) at downstream end of cavity #30 located just before the quadrupole Q2 (top) and energy spectra at both ends of the quadrupole Q2 calculated with the new solver (bottom).

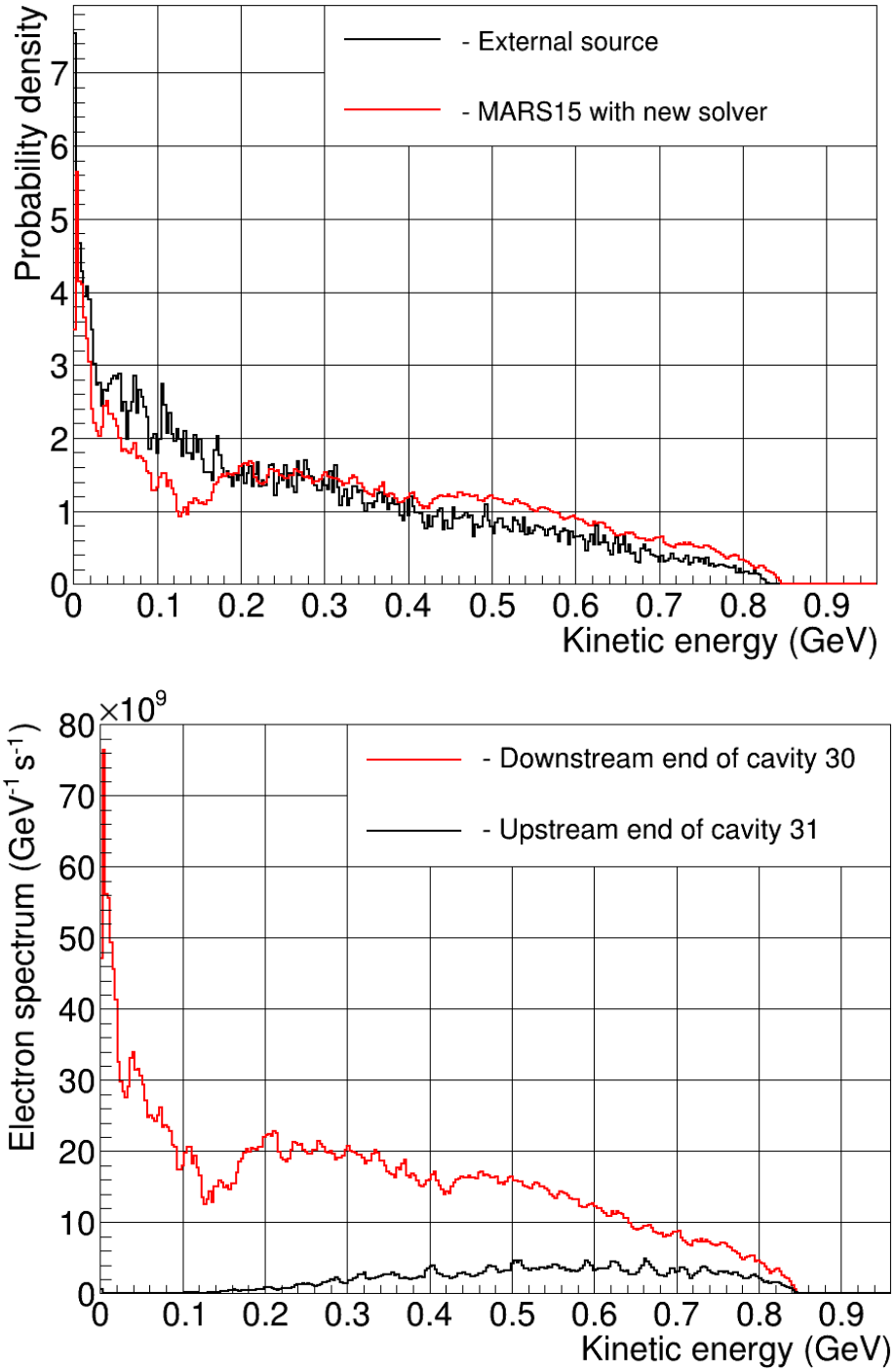

Figure 14: Partial contributions of electrons emitted from the upstream cavities to forward current at downstream end of cavity #30 (top) and distribution of heat load linear density in four cryomodules (bottom).

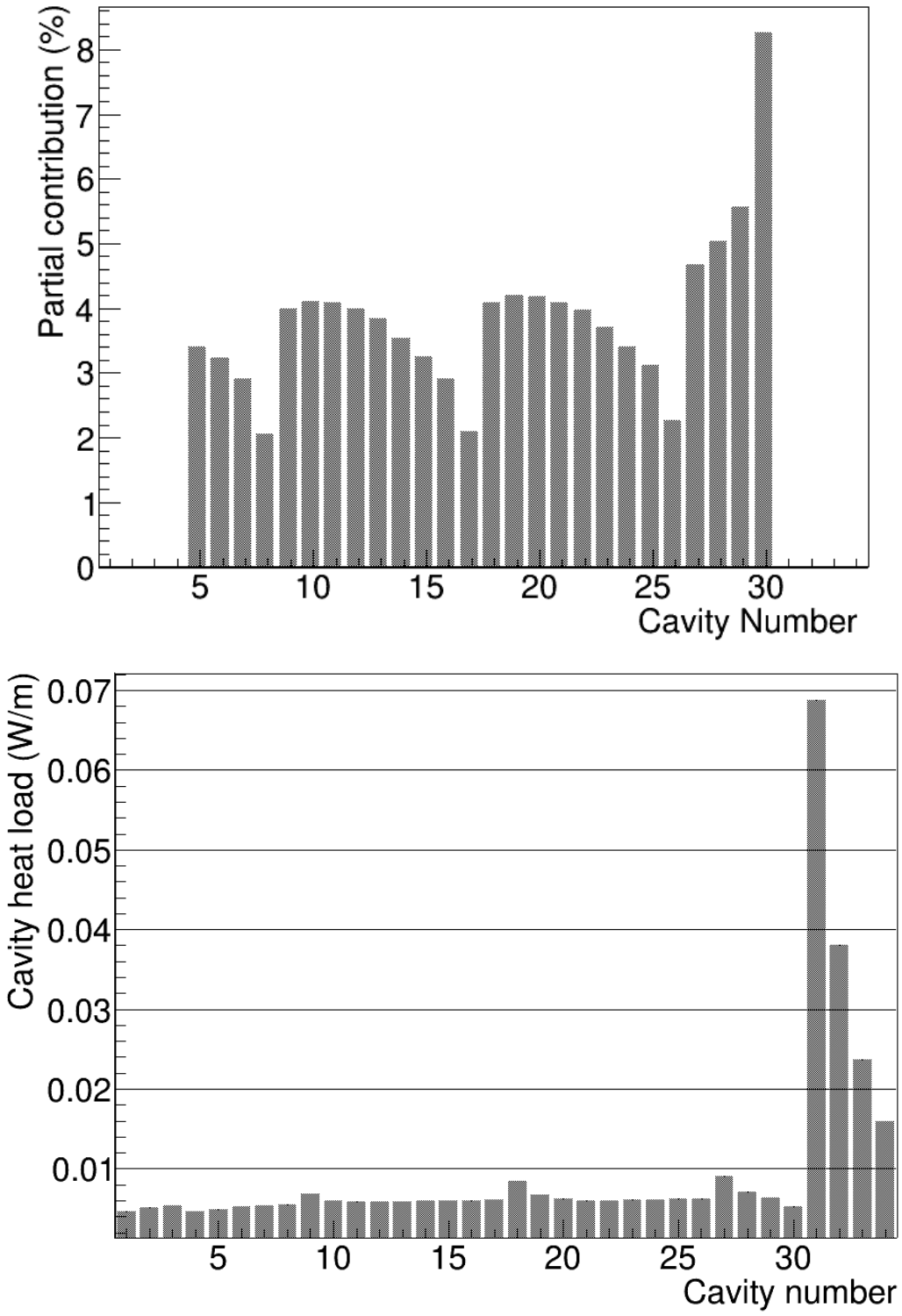

Figure 15: Calculated for the normal operation distributions of prompt dose (mSv/hr) for the beam line segment with four cryomodules: elevation view (top) and plan view (bottom).

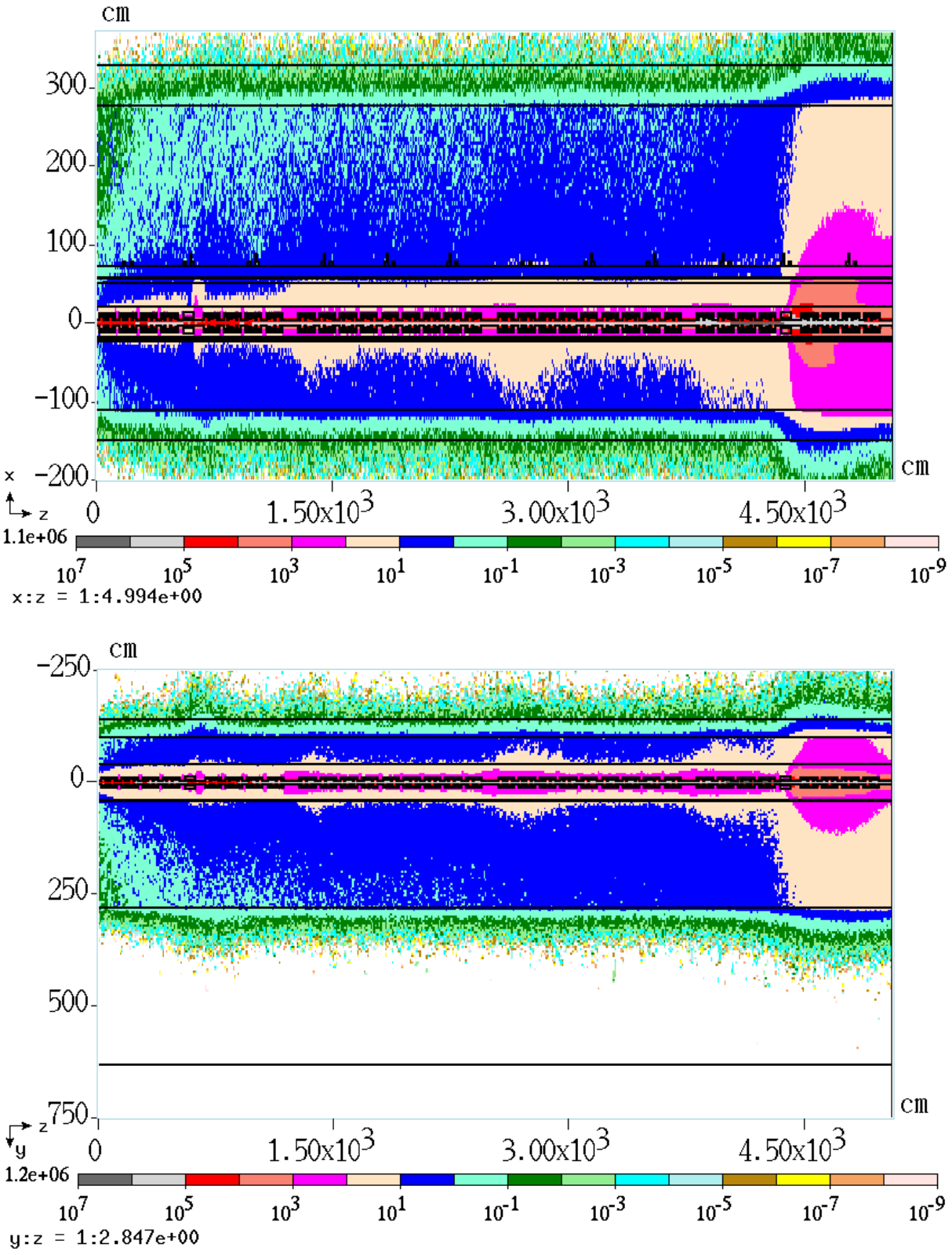

Figure 16: Calculated for the normal operation distributions of prompt dose (mSv/hr) (top) and absorbed dose (Gy/yr) (bottom) for the beam line segment with four cryomodules. The cross section is shown for the hottest spot downstream of the quadrupole magnet Q2.

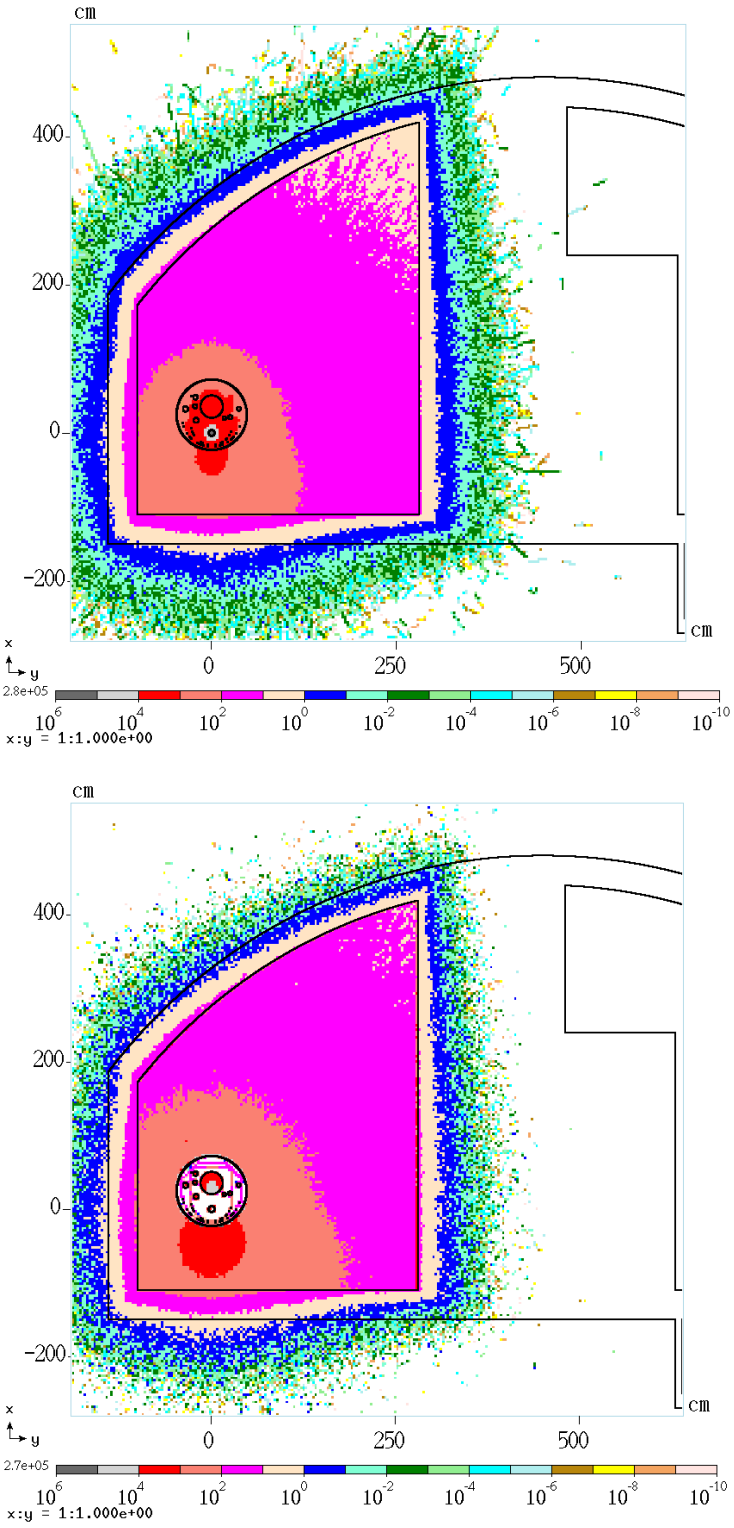

Figure 17: Calculated for the normal operation distributions of prompt dose (mSv/hr) (top) and absorbed dose (Gy/yr) (bottom) over a cross section of the cryomodule in the hottest spot downstream of the quadrupole magnet Q2.

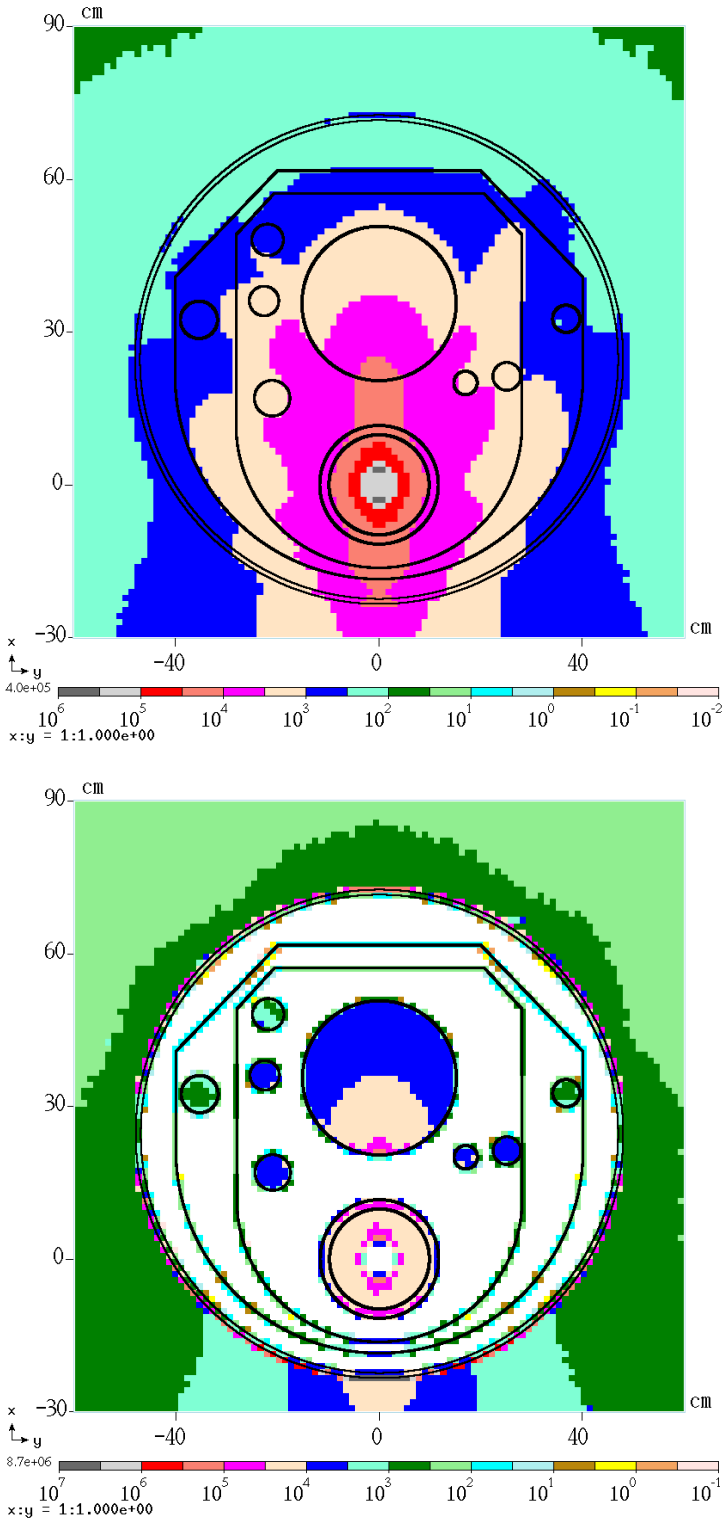

Figure 18: Calculated for the normal operation distributions of absorbed (Gy/yr) (top) and power density (mW/cm^3) (bottom) over a cross section in the hottest spot of the quadrupole magnet Q2.

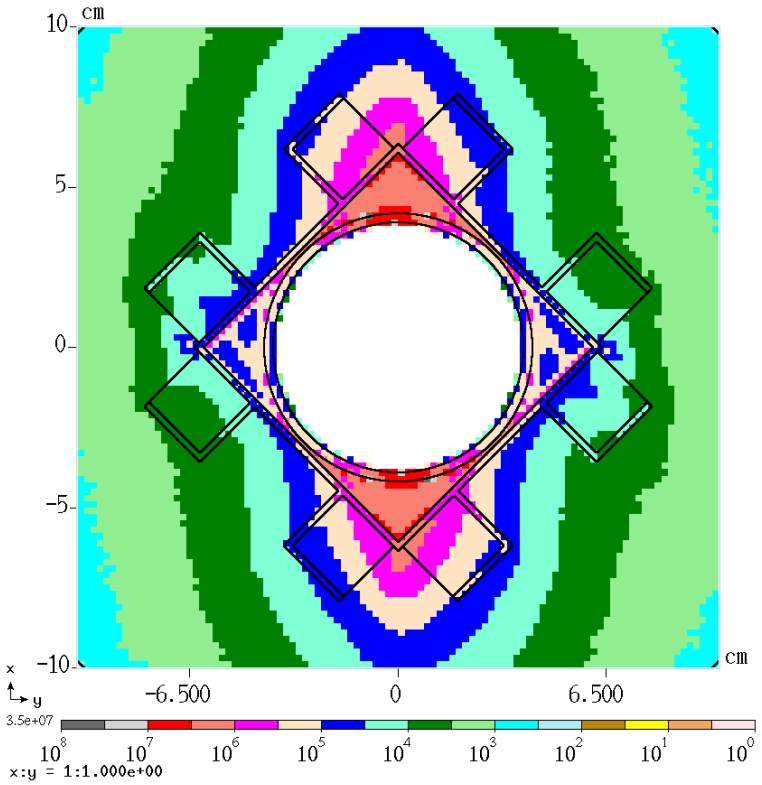

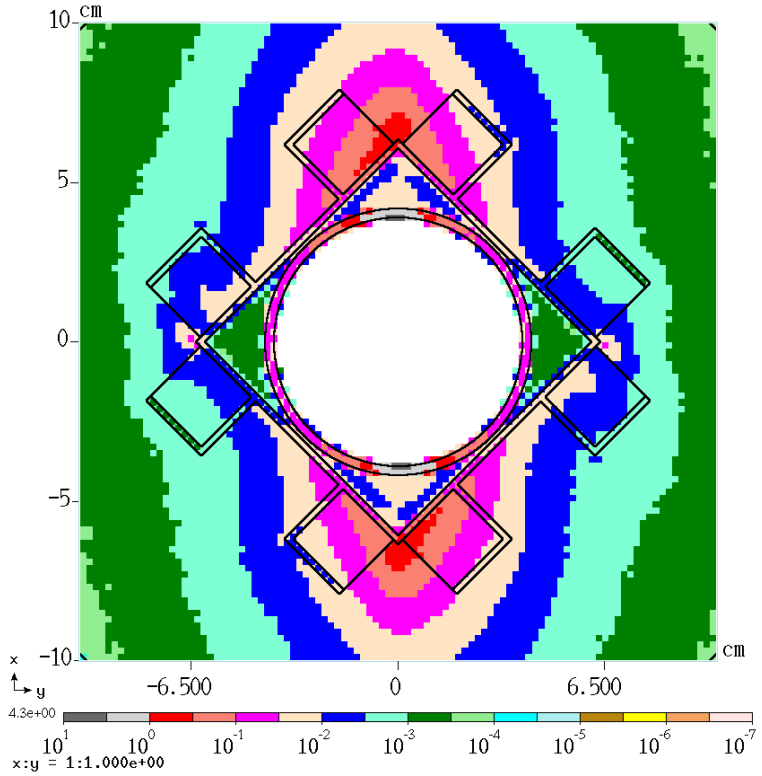

Conclusions

Radiation loads calculated for cryogenic thermometers and other elements of the ILC main linac cryomodules are substantially higher than established limits [9]. Prompt and residual dose maps across the main and service tunnels calculated for the worst-case scenario (commissioning mode) are consistent with those obtained previously in [6] confirming the 2.2-m choice for the thickness of the concrete wall between the tunnels. The radiation levels for normal operation are substantially lower. A newly developed approach for the consistent DC generation and transport agrees with the standard one with a pre-calculated source.

Results of the calculations reveal that, for approximately half of the entire linac tunnel, the radiation environment is practically independent of the longitudinal position. The major contribution to prompt dose behind the tunnel wall is due to secondary neutrons. The worst-case scenario is a commissioning mode with focusing magnets turned off and both steering and correcting magnets are on. In this case, the prompt dose at the surface of the wall in the main tunnel is approximately 2000 mSv/hr, and the dose drops to the design level of 25 μSv/hr after 2.2 m of the concrete wall.

The assumption about the maximum DC of 50 nA in each cavity was used for normalization. According to results of detailed DC modelling, this assumption is not quite adequate for a comprehensive and detailed prediction of radiation environment around the ILC main Linac tunnel. Therefore, further detailed studies are necessary in order to address the normalization issue and develop a more realistic scenario for prediction of the radiation environment in the ILC-type machines.

Acknowledgements

The authors are grateful to D. Denisov for enthusiastic support and useful discussions and A. Sukhanov for collaboration and help at early stage of this work.

This document was prepared using the resources of the Fermi National Accelerator Laboratory (Fermilab), a U.S. Department of Energy, Office of Science, HEP User Facility. Fermilab is managed by Fermi Research Alliance, LLC (FRA) acting under contract No. DE-AC02-07CH11359.

This research used a computing award allocation from the ASCR Leadership Computing Challenge at the Argonne Leadership Computing Facility, which is a DOE Office of Science User Facility supported under Contract DE-AC02-06CH11357.

References

[1] V. Balandin, et al., “Studies of Electromagnetic Cascade Showers Development in the TESLA Main Linac Initiated by Electron Field Emission in RF Cavities”, TESLA Report 2003-10.

[2] C. Pagani, “About the Dark Current Concern for TESLA”, ITRP Meeting Five, Caltech, Pasadena, 28 June 2004.

[3] N. Solyak, et al. “Dark Current Model For Ilc Main Linac”, EPAC08 (MOPP036).

[4] Y. Li, et al., “Research On Field Emission And Dark Current In ILC Cavities”, SRF2013 (TUIOA06).

[5] K. Kubo, “ML Particle Loss in Normal Operation (Beam-Gas Scattering and Dark Current”, Private communication, July 11, 2014.

[6] N. V. Mokhov, I. L. Rakhno, N. A. Solyak, A. Sukhanov, I. S. Tropin, “Dark current and radiation shielding studies for the ILC main linac,” Fermilab-Conf-16-542-APC-TD (2016).

[7] N. V. Mokhov, "*The MARS Code System User's Guide*", Fermilab-FN-628 (1995); https://mars.fnal.gov/ .

[8] N. V. Mokhov, *et al*. (2014), "MARS15 Code Developments Driven by the Intensity Frontier Needs", *Prog. Nucl. Sci. Tech.,* 4, pp. 496-501.

[9] S. Scott Courts and C. J. Yeager, "Gamma radiation induced calibration shift in four cryogenic thermometer models," *Advances in Cryogenic Engineering*, Vol. 49, American Institute of Physics, NY (July 2004).

[10] R. H. Fowler and L. Nordheim (1928), "Electron emission in intense electric fields", *Proc. Roy. Soc. London*, A119, pp. 173-181.

[11] R.G. Forbes, J.H.B. Deane (2007), "Reformulation of the standard theory of Fowler–Nordheim tunnelling and cold field electron emission," *Proceedings of the Royal Society,* A463 (2087), pp. 2907–2927.

[12] W. H. Press, S. A. Teukolsky, W. T. Vetterling, "Numerical Recipes 3rd Edition: The Art of Scientific Computing," Cambridge University Press, 3rd Edition, 2007.

[13] http://headmyshoulder.github.io/odeint-v2/

[14] A. Sukhanov, *et al.* (2015), "Model of Dark Current in SRF Linac", *Proc. 6th Int. Particle Accelerator Conf. (IPAC'15)*, Richmond, Virginia, USA, May 3-8, 2015, TUPJE081; A. Sukhanov, *et al.* (2016), "Dark current studies in ILC main linac", *Proc. 28th Linac Accelerator Conf. (LINAC16)*, East Lansing, Michigan, USA, September 25-30, 2016, THPLR007.